

The $H \rightarrow b\bar{s}$ decay and its implication for the vector-like singlet fermion model

Jin Zhang*

Department of Physics, Yuxi Normal University, Yuxi, Yunnan, 653100, China

Hong-Ying Jin[†]

*Institute of Modern Physics, School of Physics,
Zhejiang University, Hangzhou, Zhejiang, 310027, China*

T.G. Steele[‡]

*Department of Physics and Engineering Physics,
University of Saskatchewan, Saskatoon, SK, S7N 5E2, Canada*

arXiv:2309.11094v2 [hep-ph] 8 May 2024

* jinzhang@yxnu.edu.cn

† jinhongying@zju.edu.cn

‡ Tom.Steele@usask.ca

Abstract

The vector-like quark model is one of the extensions of the standard model (SM) of particle physics. The simplest version of this model introduces a vector-like singlet quark which can mix with SM quarks and give rise to new contributions to the flavor-changing decays of the Higgs boson. In this work we first present a systematic analysis of the branching ratios of the decays $H \rightarrow b\bar{s}, b\bar{d}$ at leading order in the standard model. Our results show that it is challenging to observe these two modes because of their small branching ratios. Then augmenting the SM with a vector-like singlet top quark, assuming the top partner only mixes with the top quark, complete one-loop contributions are taken into account in the amplitudes. Further results indicate that the branching ratios of the decays $H \rightarrow b\bar{s}, b\bar{d}$ are sensitive to the mass of the top partner M_T and the mixing effects characterized by $\sin\theta_L$. By tuning the values of M_T and $\sin\theta_L$, the branching ratios may rise to a level accessible to LHC experiments. Combined with the branching ratios obtained from a probabilistic model, the allowed areas in the $M_T - \sin\theta_L$ plane are displayed. Tagging efficiencies and feasibility for detecting $H \rightarrow b\bar{s}$ are specifically discussed and we conclude that with large statistics it is promising to discover the $H \rightarrow b\bar{s}$ decay at the LHC.

PACS numbers:

I. INTRODUCTION

The discovery of the long-awaited Higgs boson of the Standard Model (SM) [3–7] by the ATLAS and by the CMS collaborations at the LHC in 2012 [1, 2] marked a milestone in particle physics. Since the first observation, substantial experimental data has been accumulated on various decays of the Higgs boson in Run I and Run II as well as the ongoing Run III of the LHC. Full study of the decays of the Higgs boson holds a prominent role in deciphering physics of the SM. It is known that a Higgs boson with mass about 125 GeV can decay to many particles in the SM [8]. We may classify the dominant decay modes of the Higgs boson into two main categories according to the final state particles. The first category is decays to vector bosons, and the second category is decays to flavor-conserving fermion pairs which can occur at tree level in the SM. Abundant events of these two main categories have been observed. On the theoretical side, these two categories of decay modes have been evaluated to higher order in perturbation theory in the SM and its supersymmetric extensions [9–15]. Since flavor-changing neutral currents (FCNC) are forbidden at tree level in the SM, at leading order in perturbation theory, quark flavor changing decays of the Higgs boson (denoted by $H \rightarrow q\bar{q}'$) are mediated via triangle diagrams. It has been widely discussed that the investigation of quark flavor-changing decays [16–21] of the Higgs boson can offer practical clues for models of new physics beyond the SM, such as two-Higgs-doublet models [22–24, 28], supersymmetric models [25–29], extra dimensions [30] and fourth generation models [31].

However, observation of the quark flavor-changing decays need high statistics. Taking the decay $H \rightarrow b\bar{s}$ as an example, a qualitative estimate shows that it is more difficult to detect it than any decay modes of the Higgs boson observed at the LHC because the amplitude of this decay is suppressed in several ways. Firstly, at leading order in the SM, the process is mediated by triangle diagrams, so the squared amplitude of the process is suppressed by G_f^3 , where G_f denotes the Fermi constant. On the other hand, the CKM elements [32, 33] will provide further suppression at the order-of-magnitude about 10^{-2} or less. Finally, with the addition of heavy quarks, the contribution stemming from the Higgs couplings to light quarks are so small that they can be neglected. But thanks to the small width of the decay $H \rightarrow b\bar{s}$, it provides an opportunity to explore effects of new physics in that a small SM background give us the chance of observing the small effects of new physics. In this sense, a comprehensive study

on the branching ratios of $H \rightarrow b\bar{s}$ and other quark flavor changing Higgs decays can provide constraints on new physics models in which new particles can contribute to the amplitudes of the quark flavor changing Higgs decays.

In the quest for the new physics beyond the SM, the vector-like fermion models have drawn much attention for decades [34–55] (see Ref. [56] and references therein for an up-to-date review on this subject). A practical version of these models may introduce a new $U'(1)$ gauge group [57], which is spontaneously broken by the vacuum expectation of a scalar field Φ , transforming as $\Phi \sim (1, 1, 0, q')$ under $SU_C(3) \times SU_L(2) \times U_Y(1) \times U'(1)$. The model contains a colored Dirac fermion transforming as $T' \sim (3, 1, 2/3, q')$ which is often referred to as a top partner. The top partner also arises in little Higgs models [58–64], topcolor models [65, 66], and top condensate models [67–70]. In principle, the top partner will mix with SM quarks, but the mixing with the first two generations is highly restricted by precision electroweak data and flavor-changing neutral processes at low energies [40]. Thus it is reasonable to assume that the top partner only mixes with the top quark. In generalized versions of these models, the vector-like fermions may be a $SU_L(2)$ doublet or triplet [71–74]. The top partner, regardless of being in singlet or in the generalized models, will introduce new contributions to the amplitude of $H \rightarrow b\bar{s}$, thereby altering the decay width at a level which may be accessible to LHC experiments. Therefore, a careful analysis on the $H \rightarrow b\bar{s}$ decay may provide an alternative approach to constraining the vector-like singlet model other than trying to test it through the top partner decays to SM particles.¹

Having noted the small SM $H \rightarrow b\bar{s}$ width and the associated potential for testing the vector-like singlet quark model by this decay process, in this paper we will present a systematic analysis of the $H \rightarrow b\bar{s}$ decay at leading order in SM and then in the vector-like singlet top partner model.² We firstly evaluate the widths and branching fractions in the SM, then the contribution of top partner to the amplitudes will be considered. We assume that the top partner only mixes with the top quark, and mixing with the first two generation quarks is neglected. Another down-type flavor-changing decay of the Higgs boson, $H \rightarrow b\bar{d}$, can also be

¹ See the summary tables in Ref. [56] for an exhaustive compilation of searches for vector-like singlet quarks by ATLAS and by CMS.

² The $H \rightarrow b\bar{s}$ decay has been analyzed in Ref. [21] based on the model of a single generation of vector-like singlet down-type quarks. One can refer to the supplementary materials of Ref. [21] for details.

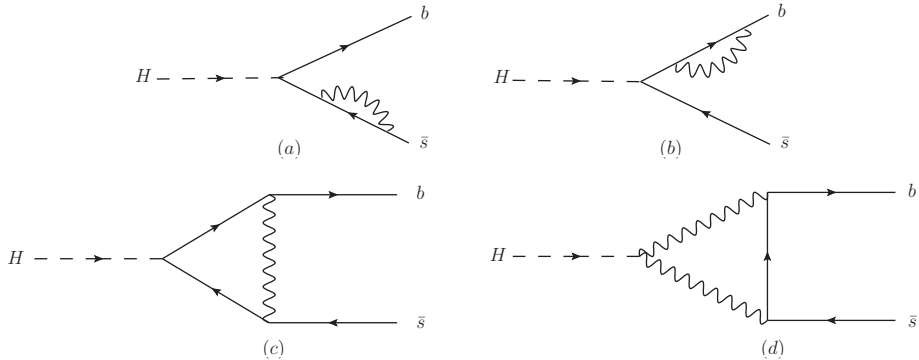


FIG. 1: One-loop diagrams contributing to the $H \rightarrow b\bar{s}$ decay in the SM.

analyzed by appropriate replacement of the parameters in the corresponding expressions.

The paper is organized as follows. In Section II the branching ratios of the processes $H \rightarrow b\bar{s}, b\bar{d}$ in the SM are evaluated, and the analytic and numerical results are presented. In Section III the contributions of the top partner are taken into account, and the role of top partner mass and mixing effects are investigated. Employing the upper bounds of the branching ratios of $H \rightarrow b\bar{s}$ from experiments and using a probabilistic model, the allowed parameter spaces are obtained. The tagging efficiencies and detection feasibility of the decay $H \rightarrow b\bar{s}$ at the LHC are discussed. Our conclusions and outlooks are summarized in Section IV. Some necessary formulae are collected in the Appendices.

II. EVALUATION THE DECAY RATE OF $H \rightarrow b\bar{s}$ IN THE STANDARD MODEL

A. the amplitude formulae

All the one-loop diagrams³ contributing to the $H \rightarrow b\bar{s}$ decay in the SM are depicted in Fig. 1. We may divide them into two groups: diagrams (a) and (b) represent quark self-energy corrections and diagrams (c) and (d) represent triangle diagrams. The amplitude of diagram

³ The Feynman diagrams in this paper are produced by Jaxodraw [75, 76].

(a) in Fig. 1 in Feynman-'t Hooft gauge is

$$M_a = -\frac{m_b(\sqrt{2}G_f)^{1/2}g_2^2}{2} \sum_q V_{qb}^* V_{qs} \int \frac{d^4k}{(2\pi)^4} \frac{1}{D_1 D_2 D_3} \\ \times \bar{u}(p_2)(\not{p}_3 + m_b)\gamma_\mu P_L(\not{p}_3 - \not{k} + m_q)\gamma^\mu P_L v(p_3), \quad (1)$$

where the summation over $q = u, c, t$ is implied, the denominators are

$$D_1 = p_3^2 - m_b^2 + i\varepsilon, \quad D_2 = k^2 - m_W^2 + i\varepsilon, \quad D_3 = (k - p_3)^2 - m_q^2 + i\varepsilon, \quad (2)$$

V_{qb}^* and V_{qs} are the elements of the CKM matrix [32, 33], and G_f is the Fermi coupling constant [8]

$$G_f = \frac{g_2^2}{4\sqrt{2}m_W^2} = 1.1664 \times 10^{-5} \text{ GeV}^{-2}. \quad (3)$$

We denote the momentum of the Higgs boson, b and \bar{s} to be p_1 , p_2 and p_3 , respectively. All the external momentum are on their mass-shell and in order to simplify the evaluation the mass of the strange quark is neglected

$$p_1^2 = m_H^2, \quad p_2^2 = m_b^2, \quad p_3^2 = m_s^2 = 0. \quad (4)$$

The equations of the motion for the bottom and the strange quarks are also needed

$$\bar{u}(p_2)\not{p}_2 = m_b\bar{u}(p_2), \quad \not{p}_3 v(p_3) = 0. \quad (5)$$

The left- and right-handed projection matrices P_L and P_R in Eq. (1) are

$$P_L = \frac{1}{2}(1 - \gamma_5), \quad P_R = \frac{1}{2}(1 + \gamma_5). \quad (6)$$

Since

$$P_L \gamma_\alpha = \gamma_\alpha P_R, \quad P_R \gamma_\alpha = \gamma_\alpha P_L, \quad (7)$$

Eq. (1) is simplified to

$$M_a = -\frac{g_2^2(\sqrt{2}G_f)^{1/2}}{m_b} \sum_q V_{qb}^* V_{qs} \int \frac{d^4k}{(2\pi)^4} \frac{\bar{u}(p_2)[-m_b\not{p}_3 + (\not{p}_3 + m_b)\not{k}]}{D_2 D_3} P_L v(p_3). \quad (8)$$

Before proceeding with the subsequent evaluation, it is necessary to illustrate that the orthogonality relation of the CKM matrix [77]

$$V_{us}V_{ub}^* + V_{cs}V_{cb}^* + V_{ts}V_{tb}^* = 0. \quad (9)$$

does not appear in Eq. (8), otherwise the whole amplitude will vanish. The reason is that since all the quarks in the propagators in Eq. (8) are massive, the integrals are different from each other, so that the coefficient of the product $V_{qs}V_{qb}^*(q = u, c, t)$ is not a common factor, and hence we get a nonzero contribution. An analogous discussion can be applied to diagrams (c) and (d) in the second row of Fig. 1.

Performing the integral in (8) using dimensional regularization [78, 79], we obtain M_a in the modified minimal subtraction ($\overline{\text{MS}}$) scheme

$$M_a = 4(\sqrt{2}G_f)^{3/2}m_W^2 \sum_q V_{qb}^*V_{qs} \left\{ [B_0(m_q) - B_1(m_q)]\bar{u}(p_2)\not{p}_1 P_L v(p_3) + [B_1(m_q) - B_0(m_q)]\bar{u}(p_2)\not{p}_2 P_L v(p_3) \right\}, \quad (10)$$

where B_0 and B_1 are the Passarino-Veltman functions [80, 81] defined in Appendix D. Imposing momentum conservation $p_1 = p_2 + p_3$ and Eq. (5), it is evident that $M_a = 0$. A similar analysis can be applied to the evaluation of diagram (b) and we also find $M_b = 0$. Thus we do not need the numerical value of B_0 and B_1 , but for completeness we provide the analytic expressions in Appendix D.

The amplitude corresponding to diagram (c) of Fig. 1 is

$$M_c = -\frac{g_2^2(\sqrt{2}G_f)^{1/2}}{2} \sum_q m_q V_{qb}^*V_{qs} \int \frac{d^4k}{(2\pi)^4} \frac{1}{D_1 D_2 D_3} \times \bar{u}(p_2)\gamma_\mu P_L (\not{k} + m_q)(\not{p}_1 - \not{k} + m_q)\gamma^\mu P_L v(p_3), \quad (11)$$

where the three denominators are given by

$$\begin{aligned} D_1 &= k^2 - m_q^2 + i\varepsilon, \\ D_2 &= (p_1 - k)^2 - m_q^2 + i\varepsilon, \\ D_3 &= (p_2 - k)^2 - m_W^2 + i\varepsilon. \end{aligned} \quad (12)$$

Carrying out the integral in Eq. (11), we can express Eq. (11) through the Passarino-Veltman function C_0

$$M_c = 4m_b m_W^2 (\sqrt{2}G_f)^{3/2} \left[\sum_q m_q^2 V_{qb}^*V_{qs} C_0(m_q, m_q, m_W) \right] \bar{u}(p_2) P_L v(p_3). \quad (13)$$

It is straightforward to write down the amplitude of diagram (d) in Fig. 1

$$M_d = -2g_2^2 m_W^2 (\sqrt{2}G_f)^{1/2} \sum_q V_{qb}^*V_{qs} \int \frac{d^4k}{(2\pi)^4} \frac{\bar{u}(p_2)(\not{k} - \not{p}_2) P_L v(p_3)}{D_1 D_2 D_3}, \quad (14)$$

where the three denominators are

$$\begin{aligned}
D_1 &= k^2 - m_W^2 + i\varepsilon, \\
D_2 &= (p_1 - k)^2 - m_W^2 + i\varepsilon, \\
D_3 &= (p_2 - k)^2 - m_q^2 + i\varepsilon.
\end{aligned} \tag{15}$$

Performing the integral over k using dimensional regularization, we obtain

$$\begin{aligned}
M_d &= -8m_b m_W^4 (\sqrt{2}G_f)^{3/2} \sum_q V_{qb}^* V_{qs} \left[C_1(m_W, m_W, m_q) + C_2(m_W, m_W, m_q) \right. \\
&\quad \left. - C_0(m_W, m_W, m_q) \right] \bar{u}(p_2) P_L v(p_3),
\end{aligned} \tag{16}$$

where the explicit expressions of C_1 and C_2 can be found in Appendix D. Combining Eqs. (13) and (16), and using Eq. (5), we obtain the following $H \rightarrow b\bar{s}$ decay amplitude at leading order in the SM

$$\begin{aligned}
M_{\text{SM}} &= M_c + M_d \\
&= 4m_b m_W^2 (\sqrt{2}G_f)^{3/2} (\mathcal{A}_1 + \mathcal{A}_2) \bar{u}(p_2) P_L v(p_3),
\end{aligned} \tag{17}$$

where the two dimensionless constants are defined as

$$\begin{aligned}
\mathcal{A}_1 &= \sum_q V_{qb}^* V_{qs} m_q^2 C_0(m_q, m_q, m_W), \\
\mathcal{A}_2 &= -2m_W^2 \sum_q V_{qb}^* V_{qs} \left[C_1(m_W, m_W, m_q) + C_2(m_W, m_W, m_q) - C_0(m_W, m_W, m_q) \right].
\end{aligned} \tag{18}$$

Summing over the spins of the b and \bar{s} for Eq. (17) yields

$$|M_{\text{SM}}|^2 = 32\sqrt{2}m_b^2 G_f^3 m_W^4 (m_H^2 - m_b^2) |\mathcal{A}_1 + \mathcal{A}_2|^2. \tag{19}$$

Then the decay width can be evaluated through the following expression

$$\Gamma(H \rightarrow b\bar{s}) = \frac{N_C(m_H^2 - m_b^2)}{8\pi m_H^3} |M_{\text{SM}}|^2, \tag{20}$$

where N_C is the number of quark colors, and the incoherent sum of the two final states $H \rightarrow b\bar{s}$ and $H \rightarrow \bar{b}s$ is considered. Replacing V_{qs} by V_{qd} in Eq. (20), we also obtain the decay width for $H \rightarrow b\bar{d}$. The other two flavor changing decays, $H \rightarrow s\bar{d}, c\bar{u}$, will be not explored in this

paper. The reason is that since we assume $m_s = 0$, the amplitude of $H \rightarrow s\bar{d}$ vanishes which can be inferred from Eq. (19) through replacing m_b by m_s . Furthermore, we do not explore the top partner effects on the $c\bar{u}$ final state because it is a next-to-leading order effect in the model used in this paper, and is hence beyond the leading-order scope of this work. Although the $c\bar{u}$ final state can be analyzed at leading order in the context of models containing down-type vector-like singlet quark, investigating models of this type is also beyond the scope the present work.

B. determination of the quark mass parameters

There are four quark masses to be fixed the Eq.(20), i.e., the masses of the u , c , t and b . Following the convention in Refs. [20, 21, 86],⁴ we use the pole mass for top quark in the numerical evaluation. While for the other three quarks, the running mass at the scale m_H will be employed in the numerical evaluation. The evolution of $\bar{m}_Q(\bar{m}_Q)$ (as given in Ref. [92]) upwards to some higher renormalization scale μ is determined by

$$\bar{m}_Q(\mu) = \bar{m}_Q(\bar{m}_Q) \frac{c\left[\frac{\alpha_s(\mu)}{\pi}\right]}{c\left[\frac{\alpha_s(\bar{m}_Q)}{\pi}\right]}, \quad (21)$$

where the functions $c(x)$ are known up to three loops [83, 84]⁵

$$\begin{aligned} c(x) &= \left(\frac{9}{2}x\right)^{4/9} (1 + 0.895x + 1.371x^2 + 1.952x^3), \quad \text{for } m_s < \mu < m_c \\ c(x) &= \left(\frac{25}{6}x\right)^{12/25} (1 + 1.014x + 1.389x^2 + 1.091x^3), \quad \text{for } m_c < \mu < m_b \\ c(x) &= \left(\frac{23}{6}x\right)^{12/23} (1 + 1.175x + 1.501x^2 + 0.1725x^3), \quad \text{for } m_b < \mu < m_t \\ c(x) &= \left(\frac{7}{2}x\right)^{4/7} (1 + 1.398x + 1.793x^2 - 0.6834x^3). \quad \text{for } m_t < \mu \end{aligned} \quad (22)$$

The analytic expression for $\alpha_s(\mu)$ is presented in Appendix A.

⁴ In Refs. [20, 21], the pole mass of the top quark is used for evaluating the branching ratio of $H \rightarrow b\bar{s}$ at leading order in SM, while in Ref. [86], the pole mass of the top quark is applied to evaluate the invariant mass distribution of $d\sigma/dm_{hh}$ in the double Higgs production process $gg \rightarrow hh$.

⁵ The evolution functions are first derived in Refs. [83, 84], here they are cited from Eq. (11) of Ref. [11].

When we apply Eq. (21) and the piecewise evolution functions in Eq. (22) to evaluate $\overline{m}_Q(m_H)$, we must cope with the threshold effects [85]. For instance, if we run $\overline{m}_c(\overline{m}_c)$ to $\overline{m}_c(m_H)$, we should carefully deal with the effects when the scale passes through $\overline{m}_b(\overline{m}_b)$. A way out of this dilemma is as follows. Since there is no threshold between $\mu = \overline{m}_b(\overline{m}_b)$ and $\mu = m_H$, we can directly obtain $\overline{m}_b(m_H)$ from $\mu = \overline{m}_b(\overline{m}_b)$ via the third function in Eq. (22). Then combined with the scale-independent ratio [92]

$$\frac{\overline{m}_b}{\overline{m}_c} = 4.584 \pm 0.007. \quad (23)$$

we can obtain $\overline{m}_c(m_H)$. The results are tabulated in Table I.

Similarly, to avoid threshold-matching issues for the u quark mass (e.g., Ref. [92] provides the u mass at a scale of 2 GeV), we again use scale-independent mass ratios. Defining

$$\overline{m}_n = \frac{\overline{m}_u + \overline{m}_d}{2}, \quad (24)$$

and by making use of the scale-independent ratios [92]

$$\xi_{cs} = \frac{\overline{m}_c}{\overline{m}_s} = 11.76_{-0.10}^{+0.05}, \quad \xi_{ud} = \frac{\overline{m}_u}{\overline{m}_d} = 0.474_{-0.074}^{+0.056}, \quad \xi_{sn} = \frac{\overline{m}_n}{\overline{m}_u} = 27.33_{-0.077}^{+0.67}, \quad (25)$$

we get

$$\frac{\overline{m}_n}{\overline{m}_u} = \frac{2\xi_{ud}}{1 + \xi_{ud}}. \quad (26)$$

Rearranging the ratio $\overline{m}_u/\overline{m}_c$ into the following form

$$\frac{\overline{m}_u}{\overline{m}_c} = \frac{\overline{m}_u}{\overline{m}_n} \frac{\overline{m}_n}{\overline{m}_s} \frac{\overline{m}_s}{\overline{m}_c} = \frac{2\xi_{ud}}{1 + \xi_{ud}} \frac{1}{\xi_{sn}} \frac{1}{\xi_{cs}} = 0.0020, \quad (27)$$

then combining with the value $\overline{m}_c(m_H)$ in Table. I, we find the running mass of up quark at scale $\mu = m_H$

$$\overline{m}_u(m_H) = 1.22 \pm 0.01 \text{ MeV}. \quad (28)$$

C. numerical results and discussion

For definiteness, we list all the masses needed in the evaluation

$$m_u(m_H) = 1.22 \pm 0.01 \text{ MeV}, \quad m_c(m_H) = 0.609_{-0.003}^{+0.006} \text{ GeV}, \quad m_b(m_H) = 2.793_{-0.016}^{+0.014} \text{ GeV}$$

$$m_t = 172.69 \pm 0.30 \text{ GeV}, \quad m_W = 80.377 \pm 0.012 \text{ GeV},$$

TABLE I: The pole masses of c and b as well as their running masses at the scale $\bar{m}_Q(\bar{m}_Q)$ and at the scale $m_H = 125.25$ GeV for $\Lambda_{\text{QCD}} = 0.208$ GeV. Ref. [92] values are used for the pole masses and $\bar{m}_Q(\bar{m}_Q)$. The unit of the masses is GeV.

Q	m_Q	$\bar{m}_Q(\bar{m}_Q)$	$\bar{m}_Q(m_H)$
c	1.67 ± 0.07	1.27 ± 0.02	$0.609_{-0.003}^{+0.006}$
b	4.78 ± 0.06	$4.18_{-0.02}^{+0.03}$	$2.793_{-0.016}^{+0.014}$

$$m_H = 125.25 \pm 0.017 \text{ GeV}, \quad (29)$$

As noted earlier, for the top quark we employ the pole mass, following the conventions of Ref. [20, 21, 86] in the evaluation the $H \rightarrow b\bar{s}$ at leading order in SM and the invariant mass distribution in $gg \rightarrow hh$ process.

The CKM elements are expressed by the Wolfenstein paramaterization [87]

$$\begin{aligned}
V_{ud} &= 1 - \frac{1}{2}\lambda^2 - \frac{1}{8}\lambda^4 + \mathcal{O}(\lambda^6), \\
V_{us} &= \lambda + \mathcal{O}(\lambda^7), \\
V_{ub} &= A\lambda^3(\rho - i\eta), \\
V_{cd} &= -\lambda + \frac{1}{2}A^2\lambda^2[1 - 2(\rho + i\eta)] + \mathcal{O}(\lambda^7), \\
V_{cs} &= 1 - \frac{\lambda^2}{2} + \frac{\lambda^4}{8}(1 + 4A^2) + \mathcal{O}(\lambda^6), \\
V_{cb} &= A\lambda^2 + \mathcal{O}(\lambda^8), \\
V_{td} &= A\lambda^3[1 - (\rho + i\eta)(1 - \frac{1}{2}\lambda^2)] + \mathcal{O}(\lambda^7), \\
V_{ts} &= -A\lambda^2 + \frac{1}{2}(1 - 2\rho)\lambda^4 - i\eta A\lambda^4 + \mathcal{O}(\lambda^6), \\
V_{tb} &= 1 - \frac{1}{2}A^2\lambda^4 + \mathcal{O}(\lambda^6),
\end{aligned} \quad (30)$$

with

$$\bar{\rho} = \rho(1 - \frac{\lambda^2}{2}), \quad \bar{\eta} = \eta(1 - \frac{\lambda^2}{2}), \quad (31)$$

The up-to-date fit of the above parameters are [92]

$$\lambda = 0.22500 \pm 0.00067, \quad A = 0.826_{-0.015}^{+0.018},$$

TABLE II: Numerical results for $\mathcal{F}_i^{\text{SM}}$ ($i = 1, 2$) in the SM using central values for all parameters.

Decay	$\mathcal{F}_1^{\text{SM}}$	$\mathcal{F}_2^{\text{SM}}$
$H \rightarrow b\bar{s}$	$-2.43 \times 10^{-6} - 4.46 \times 10^{-8}i$	$-4.00 \times 10^{-6} - 1.61 \times 10^{-7}i$
$H \rightarrow b\bar{d}$	$4.68 \times 10^{-7} - 1.22 \times 10^{-7}i$	$5.87 \times 10^{-7} - 6.61 \times 10^{-7}i$

$$\bar{\rho} = 0.159 \pm 0.010, \quad \bar{\eta} = 0.348 \pm 0.010. \quad (32)$$

Taking the central values of the parameters in the expressions for \mathcal{A}_1 and \mathcal{A}_2 , we can compare their contribution to the total amplitude of the SM. Defining

$$\mathcal{F}_i^{\text{SM}} = 4m_b m_W^2 (\sqrt{2}G_f)^{3/2} \mathcal{A}_i, \quad i = \{1, 2\}, \quad (33)$$

leads to the results in Table II. The values of $\mathcal{F}_1^{\text{SM}}$ and $\mathcal{F}_2^{\text{SM}}$ indicate that the main contribution for both decays are from diagram (d) which can be understood because the g_{Hff} coupling is less than the g_{HWW} coupling. Substituting all the parameters into Eq. (20), we obtain the following SM Higgs decay width at the scale $\mu = m_H$ for the two decays⁶

$$\Gamma(H \rightarrow b\bar{s}) = 6.17 \times 10^{-7} \text{ MeV}, \quad \Gamma(H \rightarrow b\bar{d}) = 2.58 \times 10^{-8} \text{ MeV}. \quad (34)$$

Combining Eq.(34) with the total width of the Higgs boson $\Gamma_H = 3.2_{-1.7}^{+2.4} \text{ MeV}$ [92], we obtain the branching fractions

$$\frac{\Gamma(H \rightarrow b\bar{s})}{\Gamma_H} = 1.93 \times 10^{-7}, \quad \frac{\Gamma(H \rightarrow b\bar{d})}{\Gamma_H} = 8.05 \times 10^{-9}, \quad (35)$$

in good agreement with the results based on the one-loop SM evaluation in Refs. [18, 20, 24, 30].⁷ The branching ratios of the two processes are lower than all the observed channels of the Higgs decay on the LHC, thus it is challenging to detect them.

We now consider the process $H \rightarrow b\bar{s}$ as specific example to explore possible ways to enhance amplitude. One obvious choice is the next-to-leading order corrections induced by QCD. But

⁶ The numerical evaluation is implemented via Mathematica: <https://www.wolfram.com/mathematica/>.

⁷ The branching ratios in Ref. [30] are evaluated in an universal extra dimension model. Unlike the four-dimensional SM and its extensions, there are more Feynman diagrams that contribute to the amplitudes of $H \rightarrow b\bar{s}, b\bar{d}$ decays due to the Kaluza-Klein (KK) excited-mode quark fields.

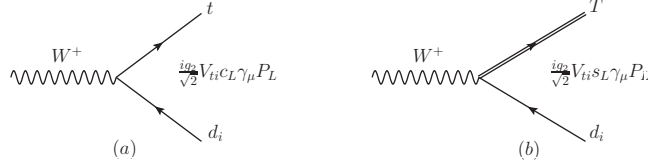


FIG. 2: Two types of couplings to W induced by the top partner.

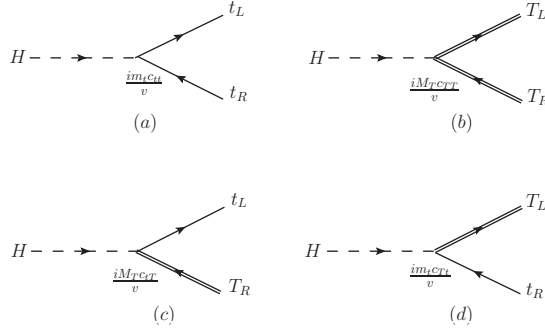


FIG. 3: Couplings of the top and its vector-like singlet partner to the Higgs boson.

at the scale of m_H where the strong coupling constant $\alpha_s \sim 0.1$, the squared amplitude will be suppressed compared to leading order. Thus we do not take it as a viable way to enhance the results in Eq. (34). Another possibility is exploring contributions from new particles. As mentioned in the introduction, the vector-like singlet fermion model is promising because the top partner also can contribute to the decay $H \rightarrow b\bar{s}$ at leading order. This implies that we can view this decay mode as a sensitive probe to explore the effects of the vector-like singlet top partner. This will be presented in the next section.

III. EVALUATING THE BRANCHING RATIOS OF THE PROCESSES $H \rightarrow b\bar{s}$, $b\bar{d}$ WITH INCLUSION OF THE VECTOR-LIKE SINGLET TOP PARTNER

A. the amplitude formulae

The Lagrangian density describing the interaction of top partner with the W^\pm is [57]

$$\mathcal{L}_W = -\frac{g_2}{\sqrt{2}} V_{ti} (c_L \bar{t} W^+ P_L d_i + s_L \bar{T} W^+ P_L d_i), +\text{h.c.} \quad (36)$$

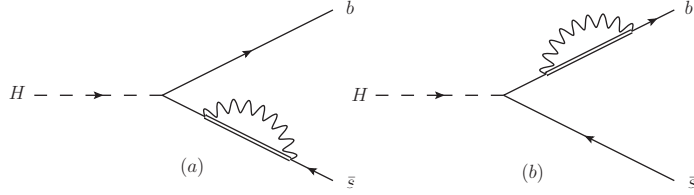


FIG. 4: The negligible one-loop diagrams with inclusion of the top partner.

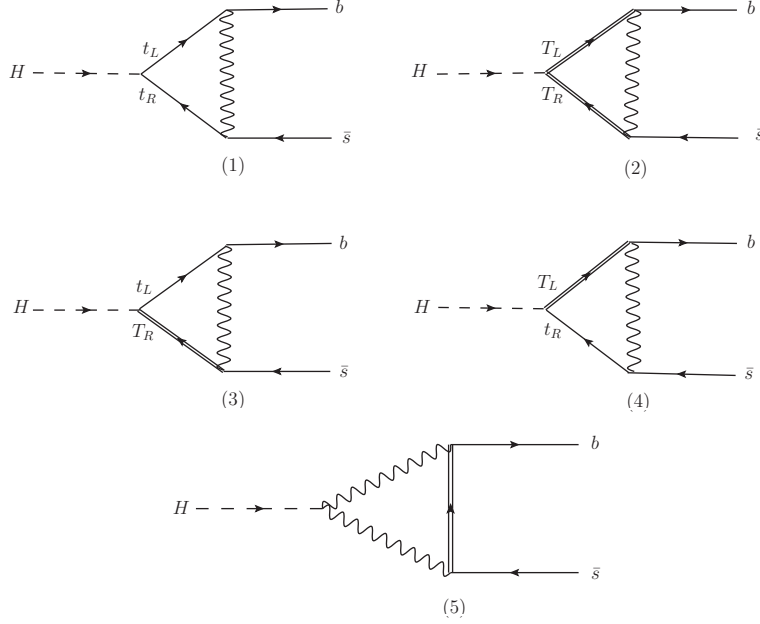


FIG. 5: One-loop diagrams contributing to $H \rightarrow b\bar{s}$ with inclusion of the top partner.

where V_{ti} ($i = d, s, b$) are the elements of the CKM matrix, and $\{c_L, s_L\}$ are respectively abbreviations for $\{\cos \theta_L, \sin \theta_L\}$. The mixing between the top quark and its singlet partner is [72, 88]

$$\begin{pmatrix} t_L \\ T_L \end{pmatrix} = \begin{pmatrix} \cos \theta_L & -\sin \theta_L \\ \sin \theta_L & \cos \theta_L \end{pmatrix} \begin{pmatrix} \mathcal{T}_L^1 \\ \mathcal{T}_L^2 \end{pmatrix}, \quad \begin{pmatrix} t_R \\ T_R \end{pmatrix} = \begin{pmatrix} \cos \theta_R & -\sin \theta_R \\ \sin \theta_R & \cos \theta_R \end{pmatrix} \begin{pmatrix} \mathcal{T}_R^1 \\ \mathcal{T}_R^2 \end{pmatrix}, \quad (37)$$

where $t_{L,R}$ and $T_{L,R}$ are the respective mass eigenstates of top quark and the top partner, while $\mathcal{T}_{R,L}^1$ and $\mathcal{T}_{R,L}^2$ are the corresponding weak eigenstates. The interactions with the SM Higgs

boson are [72]

$$\mathcal{L} = -\frac{m_t}{v}c_{tt}\bar{t}_L t_R h - \frac{M_T}{v}c_{TT}\bar{T}_L T_R h - \frac{M_T}{v}c_{tT}\bar{t}_L T_R h - \frac{m_t}{v}c_{Tt}\bar{T}_L t_R h + \text{h.c.}, \quad (38)$$

with

$$c_{tt} = c_L^2, \quad c_{TT} = s_L^2, \quad c_{tT} = c_{Tt} = s_L c_L, \quad (39)$$

From Eq. (36) and Eq. (38), we can obtain six new types of vertices which are depicted in Fig. 2 and in Fig. 3. At leading order, the diagrams contributing to the amplitude of $H \rightarrow b\bar{s}$ are depicted in Fig. 4 and in Fig. 5. By using the equation of motion of the s quark, we conclude that the contributions from the diagrams in Fig. 4 vanish, so the top partner contributes to the amplitude through the diagrams in Fig. 5.

The amplitude of the first diagram in Fig. 5 is

$$M_1 = \frac{g_2^2 m_t}{2v} V_{tb}^* V_{ts} c_{tt} c_L^2 \int \frac{d^4 k}{(2\pi)^4} \frac{\bar{u}(p_2) \gamma_\mu \gamma_L (\not{k} + m_t) P_R (\not{p}_1 - \not{k} + m_t) \gamma^\mu P_L v(p_3)}{D_1 D_2 D_3}, \quad (40)$$

where the denominators are

$$\begin{aligned} D_1 &= k^2 - m_t^2 + i\varepsilon, \\ D_2 &= (p_1 - k)^2 - m_t^2 + i\varepsilon, \\ D_3 &= (p_2 - k)^2 - m_W^2 + i\varepsilon. \end{aligned} \quad (41)$$

By employing Eq. (7), we obtain

$$M_1 = g_2^2 \frac{m_t^2}{v} V_{tb}^* V_{ts} c_{tt} c_L^2 \int \frac{d^4 k}{(2\pi)^4} \frac{\bar{u}(p_2) \not{k} P_L v(p_3)}{D_1 D_2 D_3}. \quad (42)$$

After integrating over the momentum using dimensional regularization, we obtain the following result

$$M_1 = 4Z_1 m_b m_W^2 (\sqrt{2}G_f)^{3/2} [C_1^{(1)}(m_t, m_t, m_W) + C_2^{(1)}(m_t, m_t, m_W)] \bar{u}(p_2) P_L v(p_3), \quad (43)$$

where the constant Z_1 is

$$Z_1 = -m_t^2 V_{tb}^* V_{ts} c_{tt} c_L^2, \quad (44)$$

we have expressed the vacuum value of the Higgs boson in terms of the Fermi coupling constant, and $C_1^{(1)}$, $C_1^{(2)}$ are the Passarino-Veltman functions listed in Appendix D. The amplitudes of the next three diagrams can be obtained in a similar manner

$$M_2 = 4Z_2 m_b m_W^2 (\sqrt{2}G_f)^{3/2} [C_1^{(2)}(M_T, M_T, m_W) + C_2^{(2)}(M_T, M_T, m_W)] \bar{u}(p_2) P_L v(p_3),$$

$$\begin{aligned}
M_3 &= 4Z_3 m_b m_W^2 (\sqrt{2}G_f)^{3/2} [C_1^{(3)}(m_t, M_T, m_W) + C_2^{(3)}(m_t, M_T, m_W)] \bar{u}(p_2) P_L v(p_3), \\
M_4 &= 4Z_4 m_b m_W^2 (\sqrt{2}G_f)^{3/2} [C_1^{(4)}(m_t, M_T, m_W) + C_2^{(4)}(m_t, M_T, m_W)] \bar{u}(p_2) P_L v(p_3),
\end{aligned} \tag{45}$$

with Z_i ($i = 2, 3, 4$) defined as

$$Z_2 = -M_T^2 V_{tb}^* V_{ts} s_L^2 c_{TT}, \quad Z_3 = -M_T^2 V_{tb}^* V_{ts} c_L s_L c_{tT}, \quad Z_4 = -m_t^2 V_{tb}^* V_{ts} c_L s_L c_{tT}. \tag{46}$$

The amplitude of the last diagram in Fig. 5 is

$$M_5 = -2g_2^2 m_W^2 \sin^2 \theta_L (\sqrt{2}G_f)^{1/2} V_{tb}^* V_{ts} \int \frac{d^4 k}{(2\pi)^4} \frac{\bar{u}(p_2)(\not{k} - \not{p}_2) P_L v(p_3)}{D_1 D_2 D_3}, \tag{47}$$

where the three denominators are

$$\begin{aligned}
D_1 &= k^2 - m_W^2 + i\varepsilon, \\
D_2 &= (p_1 - k)^2 - m_W^2 + i\varepsilon, \\
D_3 &= (p_2 - k)^2 - M_T^2 + i\varepsilon,
\end{aligned} \tag{48}$$

Completing the integral over k using dimensional regularization, we obtain

$$M_5 = 4Z_5 m_b m_W^2 (\sqrt{2}G_f)^{3/2} \bar{u}(p_2) P_L v(p_3), \tag{49}$$

where Z_5 is given by

$$\begin{aligned}
Z_5 &= -2m_W^2 \sin^2 \theta_L V_{tb}^* V_{ts} \left[C_1^{(5)}(m_W, m_W, M_T) + C_2^{(5)}(m_W, m_W, M_T) \right. \\
&\quad \left. - C_0^{(5)}(m_W, m_W, M_T) \right].
\end{aligned} \tag{50}$$

We can now form the total contributions from the top partner to the amplitude of the process $H \rightarrow b\bar{s}$

$$M_{\text{VL}} = \sum_{i=1}^5 M_i = 4m_b m_W^2 (\sqrt{2}G_f)^{3/2} \left(\sum_{i=1}^5 \mathcal{C}_i \right) \bar{u}(p_2) P_L v(p_3), \tag{51}$$

where the coefficients \mathcal{C}_i are given by

$$\begin{aligned}
\mathcal{C}_i &= Z_i [C_1^{(i)} + C_2^{(i)}], \quad i = 1, 2, 3, 4 \\
\mathcal{C}_5 &= Z_5 \left[C_1^{(5)}(m_W, m_W, M_T) + C_2^{(5)}(m_W, m_W, M_T) - C_0^{(5)}(m_W, m_W, M_T) \right],
\end{aligned} \tag{52}$$

and for brevity the mass dependence in $C_1^{(i)}$ and $C_2^{(i)}$ has been suppressed. Combining this result with Eq. (17) yields the total amplitude

$$M_{\text{tot}} = M_{\text{SM}} + M_{\text{VL}}$$

TABLE III: Values of $\mathcal{F}_i^{\text{VL}}$ ($i = 1, 2, \dots, 5$) for $H \rightarrow b\bar{s}$ decay for $M_T = 1500 \text{ GeV}$ and $\sin \theta_L = 0.02$, with central values for all other parameters.

Coefficient	Value
$\mathcal{F}_1^{\text{VL}}$	$-3.23 \times 10^{-8} - 5.94 \times 10^{-10}i$
$\mathcal{F}_2^{\text{VL}}$	$-1.19 \times 10^{-7} - 2.19 \times 10^{-9}i$
$\mathcal{F}_3^{\text{VL}}$	$-2.99 \times 10^{-4} - 5.48 \times 10^{-6}i$
$\mathcal{F}_4^{\text{VL}}$	$-3.95 \times 10^{-6} - 7.26 \times 10^{-8}i$
$\mathcal{F}_5^{\text{VL}}$	$-1.72 \times 10^{-6} - 3.17 \times 10^{-8}i$

$$= 4m_b m_W^2 (\sqrt{2}G_f)^{3/2} \left(\mathcal{A}_1 + \mathcal{A}_2 + \sum_{i=1}^5 \mathcal{C}_i \right) \bar{u}(p_2) P_L v(p_3). \quad (53)$$

Summing over the spins of the final quarks, we arrive at

$$|M_{\text{tot}}|^2 = 32\sqrt{2}m_b^2 G_f^3 m_W^4 (m_H^2 - m_b^2) \left| \mathcal{A}_1 + \mathcal{A}_2 + \sum_{i=1}^5 \mathcal{C}_i \right|^2. \quad (54)$$

Substituting Eq. (54) into Eq. (20), we can analyze the effects of the top partner on the $H \rightarrow b\bar{s}$ branching ratio. Finally, we note that the total amplitude of the $H \rightarrow b\bar{d}$ can be obtained by replacing V_{ts} by V_{td} in Eq. (54).

B. numerical results and discussion

In order to investigate mixing effects on the branching ratios of the process $H \rightarrow b\bar{s}$ the branching ratios as a function of M_T for selected values $\sin \theta_L = \{0.04, 0.06, 0.08\}$ are shown in the left panel of Fig. 6. Conversely, the branching ratios as a function of $\sin \theta_L$ for selected values $M_T = \{1200, 1400, 1600 \text{ GeV}\}$ are presented in the right panel of Fig. 6. Similarly, results for $H \rightarrow b\bar{d}$ are presented in Fig. 7. It is obvious that the branching ratios of both decays rise quickly with M_T or $\sin \theta_L$. This behavior occurs because the couplings of the top partner to the top quark and the Higgs boson as well as to W are proportional to the product of $\sin \theta_L$ and M_T , which can largely compensate for the suppression caused by G_f and the CKM matrix. As a result, the amplitude grows rapidly, leading to a sizeable increase in the branching ratios. It is

TABLE IV: Values of $\mathcal{F}_i^{\text{VL}}$ ($i = 1, 2, \dots, 5$) for the process $H \rightarrow b\bar{d}$ for $M_T = 1500 \text{ GeV}$ and $\sin \theta_L = 0.02$, with central values for all other parameters.

Coefficient	Value
$\mathcal{F}_1^{\text{VL}}$	$6.22 \times 10^{-9} - 1.62 \times 10^{-9}i$
$\mathcal{F}_2^{\text{VL}}$	$2.29 \times 10^{-8} - 5.98 \times 10^{-9}i$
$\mathcal{F}_3^{\text{VL}}$	$5.73 \times 10^{-5} - 1.49 \times 10^{-5}i$
$\mathcal{F}_4^{\text{VL}}$	$7.60 \times 10^{-7} - 1.98 \times 10^{-7}i$
$\mathcal{F}_5^{\text{VL}}$	$3.32 \times 10^{-7} - 8.65 \times 10^{-8}i$

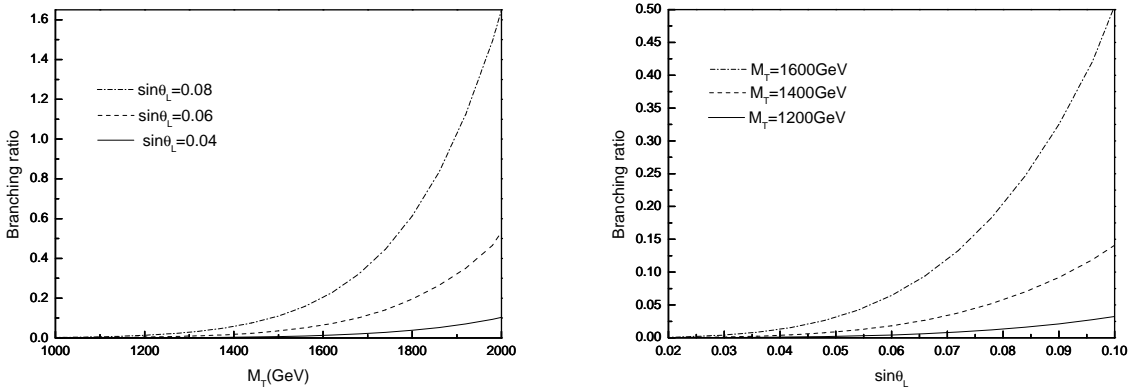


FIG. 6: The $H \rightarrow b\bar{s}$ branching ratios as a function of the mass of the vector-like top partner with selected $\sin \theta_L$ values (left) and as a function of the mixing angle with selected M_T values (right).

evident that the branching ratios of both channels could therefore increase to an level accessible to LHC experiments. For instance, taking $M_T = 1200 \text{ GeV}$ and $\sin \theta_L = 0.025$, the $H \rightarrow b\bar{s}$ decay width is about 435 eV , translating to the branching ratio is 1.36×10^{-4} , comparable to the LHC observation of $H \rightarrow \mu^+ \mu^-$ [8].

To compare the relative contribution of each diagram in Fig. 5, we list the values

$$\mathcal{F}_i^{\text{VL}} = 4m_b m_W^2 (\sqrt{2}G_f)^{3/2} \mathcal{C}_i, \quad i = 1, 2, \dots, 5 \quad (55)$$

for $H \rightarrow b\bar{s}$ and for $H \rightarrow b\bar{d}$ for $M_T = 1500 \text{ GeV}$, $\sin \theta_L = 0.02$ in Table III and Table IV,

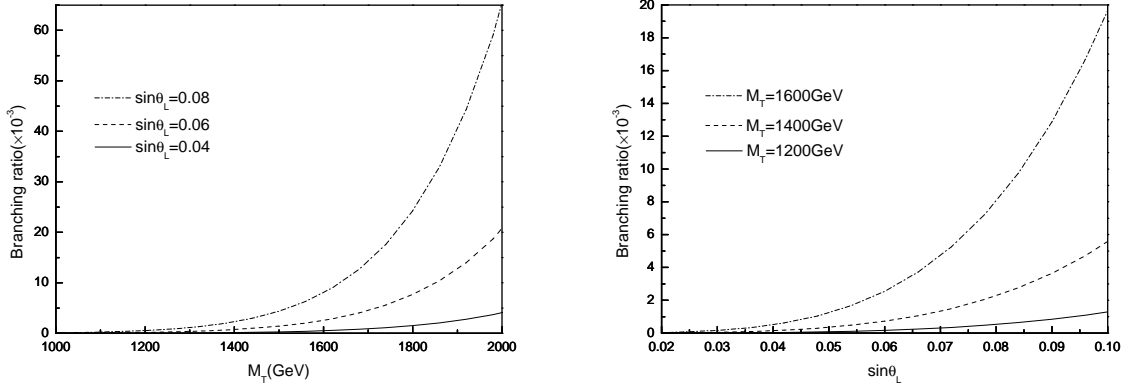


FIG. 7: The branching ratios of $H \rightarrow b\bar{d}$ as a function of the mass of the vector-like top partner with selected $\sin \theta_L$ values (left) and as a function of the mixing angle with selected M_T values (right).

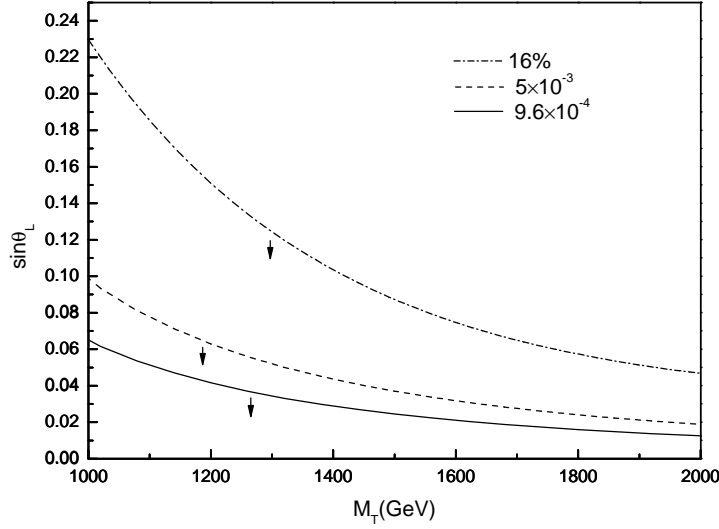


FIG. 8: The allowed region of $\{M_T, \sin \theta_L\}$ parameter space determined from different $H \rightarrow b\bar{s}$ branching ratios upper bounds. For each choice of the branching ratio, the allowed area is below the line as depicted by the arrow.

respectively. The results indicate that the third diagram in Fig. 5 is the dominant contribution to the amplitude in Eq. (51).

It is foreseeable that if we increase both M_T and $\sin \theta_L$ simultaneously or solely one of them, the evaluated $H \rightarrow b\bar{s}$ width will exceed the total width of the Higgs boson. For example, with $\sin \theta_L = 0.08$, the left panel of Fig. 6 shows that the branching ratio exceeds 100% for $M_T > 1900\text{GeV}$. The situation is not physical and must be excluded. In other words, the $H \rightarrow b\bar{s}$ branching fraction provides stringent constraints on the $\{M_T, \sin \theta_L\}$ parameter space. The analysis in Ref. [21] proposes three different upper bounds on the $H \rightarrow b\bar{s}$ branching ratios. The first one is from Higgs boson studies at the LHC [93, 94], imposing an upper limit on undetermined decays $\text{Br}(H \rightarrow \text{undet}) < 0.16$ at the 95% confidence level (CL). The second is based on a probabilistic model and if only the b -tagger is used, the upper bound $\text{Br}(H \rightarrow b\bar{s}) < 5 \times 10^{-3}$ is obtained at the 95% CL. If both the b -tagger and s -tagger are considered in the probabilistic model, the upper limit lowered to $\text{Br}(H \rightarrow b\bar{s}) < 9.6 \times 10^{-4}$ at the 95% CL. Since at present there is no direct experimental data on $H \rightarrow b\bar{s}$, it is advisable to take the three upper limits as inputs to constrain the allowed $\{M_T, \sin \theta_L\}$ parameter space as presented in Fig. 8. It is evident that a lower branching ratio bound leads to a smaller area of allowed allowed $\{M_T, \sin \theta_L\}$ parameter space. Since the upper limit 16% incorporates all the contributions from undetermined decays of the Higgs boson, we conclude that if the mass of the vector-like top partner is less than 2000 GeV, then $\sin \theta_L$ is less than 0.24.

An important issue we would like to address is the tagging efficiencies in the observation of $H \rightarrow b\bar{s}$. In this decay there are two jets in the final state. To single out the $b\bar{s}$ final state, b -tagging and s -tagging are indispensable. We may follow the techniques of the probabilistic model proposed in Ref. [21]. Applying the b -tagger and s -tagger to the two jets, the events are distributed in $(n_b, n_s) \in \{(0, 0), (1, 0), (0, 1), (2, 0), (1, 1), (0, 2)\}$ bins, where n_b and n_s denotes the numbers of b -tagger and s -tagger in the events, respectively. The b -tagger and s -tagger efficiencies are denoted by the parameters ϵ_β^b and ϵ_β^s where $\beta = \{g, s, c, b\}$ labels the flavor of the initial parton. The signal of the $H \rightarrow b\bar{s}$ decay mostly populates the (1, 1) bin while the other five bins constrain the backgrounds. In order to scan over possible tagger efficiencies, we assume $\epsilon_b^b = \epsilon_s^s$ (true positive rate, TPR) and $\epsilon_{gsc}^b = \epsilon_{gcb}^s$ (false positive rate, FPR). Then the upper bounds of the $H \rightarrow b\bar{s}$ branching ratio can be expressed as function of TPR and FPR, allowing the observation of $H \rightarrow b\bar{s}$ at the LHC. By this approach, the working point (TPR,

FPR) = (0.80, 0.004) leads to the upper bound $\text{Br}(H \rightarrow b\bar{s}) < 9.6 \times 10^{-4}$. This bound is close to the branching ratio of $H \rightarrow \mu^+\mu^-$ observed by LHC. According to the correlations between $H \rightarrow b\bar{s}$ and $B_s \rightarrow \mu^+\mu^-$ given in Ref. [95], it is possible to detect this decay at the LHC. On the other hand, the b -tagging channel $H \rightarrow b\bar{b}$ has been observed at the LHC with the branching ratio 53% [96, 97], it is the background for $H \rightarrow b\bar{s}$ and vice versa. Therefore, if the b -tagger and s -tagger efficiencies can be increased, isolating the signal of $H \rightarrow b\bar{s}$ is feasible. However, considering the hadronic noise at the LHC, the ILC [99] may provide a better environment for discovering $H \rightarrow b\bar{s}$.

C. extension to $H \rightarrow \gamma\gamma, Z\gamma$ and two-doublet vector-like quark model

Similar to $H \rightarrow b\bar{s}$, the two decays $H \rightarrow \gamma\gamma, Z\gamma$ are also affected by the presence of a singlet vector-like top partner at leading order and have been investigated in Refs. [45, 49, 72]. The model in Ref. [72] is in line with our model in this work, and the results show that the deviation of the following ratio

$$R = \frac{\text{Br}(H \rightarrow \gamma\gamma)_{\text{VL}}}{\text{Br}(H \rightarrow \gamma\gamma)_{\text{SM}}}, \quad (56)$$

from 1 is always less than 1% for small mixing ($\sin\theta_L < 0.20$) at $M_T = 1 \text{ TeV}$. Within the framework of a type-II two-Higgs doublet model embedding the vector-like singlet top partner, in Refs. [45] the two processes $H \rightarrow \gamma\gamma, Z\gamma$ are investigated. Results indicate that in order to be compatible with the observed branching ratios of these two decays, taking the value $M_T = 1 \text{ TeV}$, the mixing angle satisfies $|\sin\theta_L| < 0.25$. While the analysis in Ref. [49] is based on a SM extension with a vector-like singlet top partner plus a real singlet scalar S , from the perturbative unitarity bounds on the Yukawa coefficients $y_{L,R}^{tT}$, the values $M_T = 400 \text{ GeV}$, $\sin\theta_L = 0.20$ should be taken to get the optimal situation. This implies that if the mass of the vector-like partner significantly surpasses 1 TeV as the value employed in our analysis, the resulting branching ratios may contradict the experimental constraints. Therefore, supposing the mass of the top partner is above 1 TeV, in order to guarantee that the branching ratios of $H \rightarrow \gamma\gamma, Z\gamma$ are consistent with present experiments, the value of $\sin\theta_L$ should be taken lower than those obtained in Refs. [45, 49].

In addition to the singlet quark model employed in this work, there are vector-like doublet and triplet models [73], where the new vector-like heavy quarks of these models can also

contribute to $H \rightarrow b\bar{s}, b\bar{d}$ and other quark flavor-changing decays of the Higgs boson. A full investigation of the effects of these models on the quark flavor changing decays of the Higgs boson will modify the main content of this work. Thus we take the vector-like doublet model as an example and briefly comment its implications for the flavor changing decay of the Higgs boson. Since the flavor changing neutral current are forbidden at tree level in the SM, the singlet top partner contributes to the process $H \rightarrow c\bar{u}$ at next-to-leading order. However, the situation will be changed in the doublet vector-like quark model. In this circumstance the Higgs boson will couple to the down-type vector-like quark B_L and B_R via the following Lagrangian [72]

$$\mathcal{L} \supset -c_{bb} \frac{m_b}{v} \bar{b}_L b_R h - c_{BB} \frac{M_B}{v} \bar{B}_L B_R h - c_{bB} \frac{m_b}{v} \bar{b}_L B_R h - c_{Bb} \frac{M_B}{v} \bar{B}_L b_R h + \text{H.c.}, \quad (57)$$

where the definition of the parameters can be found in Eq. (51) of Ref. [72]. In this case we can explore the effects of the vector-like down-type quark to the decay $H \rightarrow c\bar{u}$ at leading order.

IV. SUMMARY

The discovery of the SM-like Higgs boson opens a new window to explore quark flavor changing processes. In this paper, we firstly presented a comprehensive analysis of the $H \rightarrow b\bar{s}$ and $H \rightarrow b\bar{d}$ branching ratios at leading order in the SM. The results agree with the existing work obtained in the SM [18, 20, 30].

Subsequently, based on the vector-like singlet top partner model, the $H \rightarrow b\bar{s}$ and $H \rightarrow b\bar{d}$ branching ratios of were evaluated. Further results indicate that by tuning the mass of the top partner and the mixing angle, the branching ratios of both channels will increase significantly to the level accessible to LHC experiments. Then combining our results with three different upper limits on the $H \rightarrow b\bar{s}$ branching ratio, the allowed (two-dimensional) $M_T - \sin \theta_L$ parameter space was determined. According to our results, assuming the top partner mass is less than 2000 GeV, the mixing angle should satisfy $\sin \theta_L < 0.24$.

Combining with a probabilistic model [21], tagging efficiencies and detection feasibility of the $H \rightarrow b\bar{s}$ decay are carefully considered. Our analysis shows that it is promising to detect $H \rightarrow b\bar{s}$ at the LHC, but high statistics is needed.

Since we only consider the singlet top partner model, the up-type flavor changing final state $c\bar{u}$ has not been taken into account, but can be included in extensions to doublet or triplet

vector-like models. Such studies will be explored in our future work.

V. ACKNOWLEDGEMENTS

TGS is grateful for research funding from the Natural Sciences and Engineering Research Council of Canada (NSERC).

Appendix A: the running of the strong coupling constant

The up-to-date results for the $\overline{\text{MS}}$ -scheme strong coupling is [92]

$$\alpha_s(M_Z) = 0.1179 \pm 0.0009, \quad (\text{A1})$$

and using the central value we obtain $\Lambda_{\text{QCD}}^{(5)} = 0.208\text{GeV}$. By employing this value, up to three-loop approximation in QCD [82, 89–91], the running of α_s at some energy scale μ can be determined

$$\alpha_s(\mu) = \frac{4\pi}{\beta_0 \ln(\mu^2/\Lambda^2)} \left\{ 1 - \frac{2\beta_1 \ln \ln(\mu^2/\Lambda^2)}{\beta_0^2 \ln(\mu^2/\Lambda^2)} + \frac{4\beta_1^2}{\beta_0^4 \ln^2(\mu^2/\Lambda^2)} \left[\left(\ln \ln \frac{\mu^2}{\Lambda^2} - \frac{1}{2} \right)^2 + \frac{\beta_2 \beta_0}{8\beta_1^2} - \frac{5}{4} \right] \right\}, \quad (\text{A2})$$

where the coefficients are given by

$$\beta_0 = 11 - \frac{2}{3}N_f, \quad \beta_1 = 51 - \frac{19}{3}N_f, \quad \beta_2 = 2857 - \frac{5033}{9}N_f + \frac{325}{27}N_f^2. \quad (\text{A3})$$

with N_f being the number of the active quarks below the scale μ .

Appendix B: the dilogarithms

The dilogarithm is defined as [100]

$$\text{Li}_2(x) = \sum_{n=1}^{+\infty} \frac{x^n}{n^2} = - \int_0^x \frac{\ln(1-t)}{t} dt, \quad |x| < 1, \quad (\text{B1})$$

and an equivalent definition is

$$\text{Li}_2(x) = - \int_0^1 \frac{\ln(1-xt)}{t} dt, \quad (\text{B2})$$

where there is a branch cut from 1 to $+\infty$,

$$\text{Li}_2(x + i\varepsilon) = \text{Re Li}_2(x) + i\pi \text{sgn}(\varepsilon)\Theta(x - 1) \ln x, \quad \varepsilon \rightarrow 0 \quad (\text{B3})$$

and the step function $\Theta(x)$ and the $\text{sgn}(x)$ are as follows

$$\Theta(x) = \begin{cases} 1, & x > 0 \\ 0, & x < 0 \end{cases} \quad (\text{B4})$$

and

$$\text{sgn}(x) = \begin{cases} 1, & x > 0 \\ -1, & x < 0 \end{cases}. \quad (\text{B5})$$

Two other useful formulae are [100]

$$\text{Li}_2(x, \theta) = \text{Re Li}_2(xe^{i\theta}) = -\frac{1}{2} \int_0^x \frac{\ln(1 - 2t \cos \theta + t^2)}{t} dt, \quad (\text{B6})$$

and

$$\text{Li}_2(x) + \text{Li}_2\left(\frac{1}{x}\right) = \frac{\pi^2}{3} - \frac{1}{2} \ln^2(x) - i\pi \ln x, \quad x > 1. \quad (\text{B7})$$

Appendix C: Useful integrals in the evaluation

The first integral frequently used in our evaluation is

$$F(a, b, c) = \int_0^1 \ln(ax^2 + bx + c - i\varepsilon) dx, \quad (\text{C1})$$

If $b^2 - 4ac > 0$, there are two zeros of the argument in the range $[0, 1]$, the logarithm can develop imaginary part, and the result is [98]

$$\begin{aligned} F(a, b, c) = & \ln(a - i\varepsilon) - 2 + (1 - x_-) \ln(1 - x_- + i\varepsilon) + x_- \ln(-x_- + i\varepsilon) \\ & + (1 - x_+) \ln(1 - x_+ - i\varepsilon) + x_+ \ln(-x_+ - i\varepsilon), \end{aligned} \quad (\text{C2})$$

where

$$x_+ = \frac{1}{2a}(-b + \sqrt{b^2 - 4ac}), \quad x_- = \frac{1}{2a}(-b - \sqrt{b^2 - 4ac}). \quad (\text{C3})$$

If $b^2 - 4ac < 0$, then the argument of the logarithm is always positive, and the result reads

$$F(a, b, c) = \ln(a + b + c - i\varepsilon) - 2 + \frac{b}{2a} \ln \frac{a + b + c - i\varepsilon}{c}$$

$$+ \frac{\sqrt{4ac - b^2}}{a} \left(\arctan \frac{2a + b}{\sqrt{4ac - b^2}} - \arctan \frac{b}{\sqrt{4ac - b^2}} \right). \quad (\text{C4})$$

The second type integral is

$$G(\alpha; a, b, c) = \int_0^1 \frac{\ln(ax^2 + bx + c - i\varepsilon)}{x + \alpha} dx. \quad (\text{C5})$$

In this case we should distinguish between three cases: $\alpha > 0$, $-1 < \alpha < 0$ and $\alpha < -1$. If $b^2 - 4ac > 0$, for the three cases of α , the result can be expressed uniformly as

$$\begin{aligned} G(\alpha; a, b, c) &= \ln |1 + \alpha| \ln(a + b + c - i\varepsilon) - \ln |\alpha| \ln(c - i\varepsilon) \\ &+ \ln \left| 1 + \frac{1}{\alpha} \right| \ln \left| \frac{a\alpha^2 - b\alpha + c}{a + b + c} \right| \\ &+ \text{Li}_2 \left[\frac{\alpha}{\alpha + x_+} - i\varepsilon \text{sgn}(\alpha) \right] - \text{Li}_2 \left[\frac{1 + \alpha}{\alpha + x_+} - i\varepsilon \text{sgn}(1 + \alpha) \right] \\ &+ \text{Li}_2 \left[\frac{\alpha}{\alpha + x_-} + i\varepsilon \text{sgn}(\alpha) \right] - \text{Li}_2 \left[\frac{1 + \alpha}{\alpha + x_-} + i\varepsilon \text{sgn}(1 + \alpha) \right]. \end{aligned} \quad (\text{C6})$$

If $b^2 - 4ac < 0$, the argument of the logarithm is always positive, and by employing Eq. (B6), we obtain

$$G(\alpha; a, b, c) = \ln D \ln \left| 1 + \frac{1}{\alpha} \right| - 2\text{Li}_2 \left(\frac{1 + \alpha}{m}, \theta \right) + 2\text{Li}_2 \left(\frac{\alpha}{m}, \theta \right) \quad (\text{C7})$$

where

$$D = a\alpha^2 - b\alpha + c, \quad m = \sqrt{\alpha^2 - \alpha \frac{b}{a} + \frac{c}{a}}, \quad \theta = \arccos \frac{2a\alpha - b}{2\sqrt{aD}}. \quad (\text{C8})$$

For numerical convenience we recast Eq. (C7) into the following form

$$G(a, b, c) = \ln D \ln \left| 1 + \frac{1}{\alpha} \right| - 2\text{Re} \text{Li}_2(x_1 e^{i\theta}) + 2\text{Re} \text{Li}_2(x_2 e^{i\theta}), \quad (\text{C9})$$

with

$$x_1 = \frac{(1 + \alpha)\sqrt{a}}{\sqrt{D}}, \quad x_2 = \frac{\alpha\sqrt{a}}{\sqrt{D}}. \quad (\text{C10})$$

Appendix D: Passarino-Veltman functions

The following two- and three-point functions are frequently needed in the evaluation of the amplitudes. By employing dimensional regularization, setting $d = 4 - 2\epsilon$, we obtain the two-point functions B_0 constrained by $p^2 = 0$

$$\mathcal{B}_0 = \int \frac{d^d k}{(2\pi)^d} \frac{1}{(k^2 - m_W^2 + i\varepsilon)[(k - p)^2 - m_q^2 + i\varepsilon]}$$

$$= \frac{i}{(4\pi)^2} \left[\frac{1}{\epsilon} - \gamma_E + \ln(4\pi) \right] + B_0(m_q) + \mathcal{O}(\epsilon), \quad (\text{D1})$$

where $\gamma_E = 0.5772\dots$ is the Euler-Mascheroni constant, and $B_0(m_q)$ is given by

$$B_0(m_q) = -\frac{i}{(4\pi)^2} \left(-1 + \ln \frac{m_W^2}{\mu^2} + \frac{m_q^2}{m_W^2 - m_q^2} \ln \frac{m_W^2}{m_q^2} \right). \quad (\text{D2})$$

The vector two-point function is

$$\begin{aligned} B_\mu &= \int \frac{d^d k}{(2\pi)^d} \frac{k_\mu}{(k^2 - m_W^2 + i\epsilon)[(k-p)^2 - m_q^2 + i\epsilon]} \\ &= \frac{ip_\mu}{32\pi^2} \left[\frac{1}{\epsilon} - \gamma_E + \ln(4\pi) \right] + B_1(m_q)p_\mu + \mathcal{O}(\epsilon), \end{aligned} \quad (\text{D3})$$

with

$$B_1(m_q) = -\frac{i}{32\pi^2} \left[-\frac{3}{2} + \ln \frac{m_W^2}{\mu^2} - \frac{m_q^2}{m_W^2 - m_q^2} + \frac{m_q^2(2m_W^2 - m_q^2)}{(m_W^2 - m_q^2)^2} \ln \frac{m_W^2}{m_q^2} \right]. \quad (\text{D4})$$

The general scalar and vector three-point functions are defined as

$$\begin{aligned} C_0(m_1, m_2, m_3, p_1^2, p_2^2) &= \int \frac{d^d k}{(2\pi)^d} \frac{1}{D_1 D_2 D_3}, \\ C_\mu(m_1, m_2, m_3, p_1, p_2) &= \int \frac{d^d k}{(2\pi)^d} \frac{k_\mu}{D_1 D_2 D_3} = C_1 p_{1\mu} + C_2 p_{2\mu}, \end{aligned} \quad (\text{D5})$$

where

$$\begin{aligned} D_1 &= k^2 - m_1^2 + i\epsilon, \\ D_2 &= (p_1 - k)^2 - m_2^2 + i\epsilon, \\ D_3 &= (p_2 - k)^2 - m_3^2 + i\epsilon. \end{aligned} \quad (\text{D6})$$

In order to express the three-point functions in a concise form, it is convenient to define the following parameters formed by the masses in the evaluation

$$\begin{aligned} a_1 &= m_H^2, & b_1 &= m_1^2 - m_H^2 - m_2^2, & c_1 &= m_2^2, \\ a_2 &= m_b^2, & b_2 &= m_1^2 - m_b^2 - m_3^2, & c_2 &= m_3^2, \\ a_3 &= m_1^2 - m_3^2, & b_3 &= c_2 = m_3^2, \\ \alpha &= \frac{m_2^2 - m_3^2}{m_b^2 - m_H^2}, & \beta &= \frac{m_3^2 - m_2^2}{m_H^2}. \end{aligned} \quad (\text{D7})$$

In the case $p_1^2 = m_H^2$, $p_2^2 = m_b^2$, the results read

$$C_0(m_1, m_2, m_3, p_1^2, p_2^2) = \frac{-i}{(4\pi)^2(m_H^2 - m_b^2)} \left[G(a_2, b_2, c_2) - G(a_1, b_1, c_1) \right], \quad (\text{D8})$$

$$\begin{aligned}
C_1(m_1, m_2, m_3, p_1^2, p_2^2) &= \frac{-i}{(4\pi)^2(m_H^2 - m_b^2)} \left\{ 1 + F(a_1, b_1, c_1) \right. \\
&- (1 + \alpha) \left[\ln \left| 1 + \frac{1}{\alpha} \right| + G(a_1, b_1, c_1) \right] \left. \right\} \\
&- \frac{i}{(4\pi)^2(m_H^2 - m_b^2)^2} \left\{ \left[\frac{c_2}{\alpha} \ln(c_2 - i\varepsilon) - \frac{a_2 + b_2 + c_2}{1 + \alpha} \ln(a_2 + b_2 + c_2 - i\varepsilon) \right. \right. \\
&+ 2a_2 \left(1 + F(a_2, b_2, c_2) \right) + (b_2 - 2\alpha a_2) \left(\ln \left| 1 + \frac{1}{\alpha} \right| + G(a_2, b_2, c_2) \right) \left. \right] \\
&- (a_2 \leftrightarrow a_1, b_2 \leftrightarrow b_1, c_2 \leftrightarrow c_1) \left. \right\} + \mathcal{O}(\epsilon), \tag{D9}
\end{aligned}$$

$$\begin{aligned}
C_2(m_1, m_2, m_3, p_1^2, p_2^2) &= \frac{-i}{(4\pi)^2(m_H^2 - m_b^2)} \left\{ -1 - F(a_2, b_2, c_2) \right. \\
&+ (1 + \alpha) \left[\ln \left| 1 + \frac{1}{\alpha} \right| + G(a_2, b_2, c_2) \right] \left. \right\} \\
&- \frac{i}{(4\pi)^2(m_H^2 - m_b^2)^2} \left\{ \left[\frac{c_1}{\alpha} \ln(c_1 - i\varepsilon) - \frac{a_1 + b_1 + c_1}{1 + \alpha} \ln(a_1 + b_1 + c_1 - i\varepsilon) \right. \right. \\
&+ 2a_1 \left(1 + F(a_1, b_1, c_1) \right) + (b_1 - 2\alpha a_1) \left(\ln \left| 1 + \frac{1}{\alpha} \right| + G(a_1, b_1, c_1) \right) \left. \right] \\
&- (a_1 \leftrightarrow a_2, b_1 \leftrightarrow b_2, c_1 \leftrightarrow c_2) \left. \right\} + \mathcal{O}(\epsilon). \tag{D10}
\end{aligned}$$

-
- [1] G. Aad *et al.* [ATLAS], Observation of a new particle in the search for the standard model Higgs boson with the ATLAS detector at the LHC, *Phys. Lett. B* **716**, 1 (2012).
- [2] S. Chatrchyan *et al.* [CMS], Observation of a new boson at a mass of 125 GeV with the CMS experiment at the LHC, *Phys. Lett. B* **716**, 30 (2012).
- [3] F. Englert and R. Brout, Broken symmetry and the mass of gauge vector mesons, *Phys. Rev. Lett.* **13**, 321 (1964).
- [4] P. W. Higgs, Broken symmetries and the masses of gauge bosons, *Phys. Rev. Lett.* **13**, 508 (1964).
- [5] P. W. Higgs, Spontaneous symmetry breakdown without massless bosons, *Phys. Rev.* **145**, 1156 (1966).
- [6] G. S. Guralnik, C. R. Hagen and T. W. B. Kibble, Global conservation laws and massless particles, *Phys. Rev. Lett.* **13**, 585 (1964).
- [7] T. W. B. Kibble, Symmetry breaking in non-Abelian gauge theories, *Phys. Rev.* **155**, 1554 (1967).

- [8] M. Carena, C. Grojean, M. Kado *et al.*, “Status of Higgs boson physics” in Ref. [92].
- [9] J. F. Gunion, H. E. Haber, G. L. Kane and S. Dawson, *The Higgs Hunter’s Guide*(Perseus Publishing, Cambridge, Massachusetts, 1990).
- [10] B. A. Kniehl, Higgs phenomenology at one loop in the standard model, *Phys. Rept.* **240**, 211 (1994).
- [11] M. Spira, QCD effects in Higgs physics, *Fortsch. Phys.* **46**, 203 (1998).
- [12] A. Djouadi, The anatomy of electro-weak symmetry breaking. I: The Higgs boson in the standard model, *Phys. Rept.* **457**, 1 (2008).
- [13] A. Djouadi, The anatomy of electro-weak symmetry breaking. II. The Higgs bosons in the minimal supersymmetric model, *Phys. Rept.* **459**, 1 (2008).
- [14] M. Spira, Higgs boson production and decay at hadron colliders, *Prog. Part. Nucl. Phys.* **95**, 98 (2017).
- [15] S. Y. Choi, J. S. Lee and J. Park, Decays of Higgs bosons in the standard model and beyond, *Prog. Part. Nucl. Phys.* **120**, 103880 (2021).
- [16] R. S. Willey and H. L. Yu, Neutral Higgs boson from decays of heavy flavored mesons, *Phys. Rev. D* **26**, 3086 (1982).
- [17] B. Grzadkowski and P. Krawczyk, Higgs particle effects in flavor changing transitions, *Z. Phys. C* **18**, 43 (1983).
- [18] L. G. Benitez-Guzmán, I. García-Jiménez, M. A. López-Osorio, E. Martínez-Pascual and J. J. Toscano, Revisiting the flavor changing neutral current Higgs decays $H \rightarrow q_i q_j$ in the Standard Model, *J. Phys. G* **42**, 085002 (2015).
- [19] D. Barducci and A. J. Helmboldt, Quark flavour-violating Higgs decays at the ILC, *JHEP* **12**, 105 (2017)
- [20] J. I. Aranda, G. González-Estrada, J. Montaño, F. Ramírez-Zavaleta and E. S. Tututi, Revisiting the rare $H \rightarrow q_i q_j$ decays in the standard model, *J. Phys. G* **47**, 125001 (2020).
- [21] J. F. Kamenik, A. Korajac, M. Szewc, M. Tammara and J. Zupan, Flavor-violating Higgs and Z boson decays at a future circular lepton collider, *Phys. Rev. D* **109**, L011301 (2024).
- [22] A. Arhrib, Higgs bosons decay into bottom-strange in two Higgs doublets models, *Phys. Lett. B* **612**, 263(2005).

- [23] A. Crivellin, J. Heeck and D. Müller, Large $h \rightarrow bs$ in generic two-Higgs-doublet models, Phys. Rev. D **97**, 035008 (2018).
- [24] F. Arco, S. Heinemeyer and M. J. Herrero, Role of $\lambda_{hH^+H^-}$ in Higgs boson decays h to bs in the 2HDM, Phys. Rev. D **108**, 095047 (2023).
- [25] S. Bejar, F. Dilme, J. Guasch and J. Sola, Higgs boson flavor changing neutral decays into bottom quarks in supersymmetry, JHEP **08**, 018 (2004)
- [26] W. Hollik, S. Penaranda and M. Vogt, Flavor changing effects on $e^+e^- \rightarrow Hb\bar{s}, H\bar{b}s$ in the MSSM, Eur. Phys. J. C **47**, 207 (2006).
- [27] A. Arhrib, D. K. Ghosh, O. C. W. Kong and R. D. Vaidya, Flavor changing Higgs decays in supersymmetry with minimal flavor violation, Phys. Lett. B **647**, 36 (2007).
- [28] G. Barenboim, C. Bosch, J. S. Lee, M. L. López-Ibáñez and O. Vives, Flavor-changing Higgs boson decays into bottom and strange quarks in supersymmetric models, Phys. Rev. D **92**, 095017 (2015).
- [29] M. E. Gómez, S. Heinemeyer and M. Rehman, Quark flavor violating Higgs boson decay $h \rightarrow \bar{b}s + b\bar{s}$ in the MSSM, Phys. Rev. D **93**, 095021 (2016).
- [30] C. M. Farrera, A. Granados-González, H. Novales-Sánchez and J. J. Toscano, Quark-flavor-changing Higgs decays from a universal extra dimension, Int. J. Mod. Phys. A **35**, 2050141 (2020).
- [31] G. Eilam, B. Haeri and A. Soni, Flavor changing Higgs transitions, Phys. Rev. D **41**, 875 (1990).
- [32] N. Cabibbo, Unitary symmetry and leptonic decays, Phys. Rev. Lett. **10**, 531 (1963).
- [33] M. Kobayashi and T. Maskawa, CP Violation in the renormalizable theory of weak interaction, Prog. Theor. Phys. **49**, 652 (1973).
- [34] F. del Aguila and J. Cortes, A new model of weak CP violation, Phys. Lett. B **156**, 243(1985).
- [35] G. C. Branco and L. Lavoura, On the addition of vector like quarks to the standard model, Nucl. Phys. B **278**, 738 (1986).
- [36] P. M. Fishbane, S. Meshkov, R. E. Norton and P. Ramond, Chiral fermions beyond the standard model, Phys. Rev. D **31**, 1119 (1985).
- [37] P. M. Fishbane, R. E. Norton and M. J. Rivard, Experimental implications of heavy isosinglet quarks and leptons, Phys. Rev. D **33**, 2632 (1986).

- [38] J. L. Hewett and T. G. Rizzo, Low-energy phenomenology of superstring inspired $E(6)$ models, *Phys. Rept.* **183**, 193 (1989).
- [39] A. Leike, The phenomenology of extra neutral gauge bosons, *Phys. Rept.* **317**, 143 (1999).
- [40] J. A. Aguilar-Saavedra, Effects of mixing with quark singlets, *Phys. Rev. D* **67**, 035003 (2003), [erratum: *Phys. Rev. D* **69**, 099901 (2004)].
- [41] J. Kang, P. Langacker and B. D. Nelson, Theory and phenomenology of exotic isosinglet quarks and squarks, *Phys. Rev. D* **77**, 035003 (2008).
- [42] G. Cacciapaglia, A. Deandrea, L. Panizzi, N. Gaur, D. Harada and Y. Okada, Heavy vector-like top partners at the LHC and flavour constraints, *JHEP* **03**, 070 (2012).
- [43] G. Cacciapaglia, A. Carvalho, A. Deandrea, T. Flacke, B. Fuks, D. Majumder, L. Panizzi and H. S. Shao, Next-to-leading-order predictions for single vector-like quark production at the LHC, *Phys. Lett. B* **793**, 206 (2019).
- [44] S. A. R. Ellis, R. M. Godbole, S. Gopalakrishna and J. D. Wells, Survey of vector-like fermion extensions of the Standard Model and their phenomenological implications, *JHEP* **09**, 130 (2014).
- [45] A. Arhrib, R. Benbrik, S. J. D. King, B. Manaut, S. Moretti and C. S. Un, Phenomenology of 2HDM with vectorlike quarks, *Phys. Rev. D* **97**, 095015 (2018).
- [46] G. Cacciapaglia, H. Cai, A. Carvalho, A. Deandrea, T. Flacke, B. Fuks, D. Majumder and H. S. Shao, Probing vector-like quark models with Higgs-boson pair production, *JHEP* **07**, 005 (2017).
- [47] J. H. Kim and I. M. Lewis, Loop induced single top partner production and decay at the LHC, *JHEP* **05**, 095 (2018).
- [48] H. Alhazmi, J. H. Kim, K. Kong and I. M. Lewis, Shedding light on top partner at the LHC, *JHEP* **01**, 139 (2019).
- [49] S. P. He, Higgs boson to γZ decay as a probe of flavor-changing neutral Yukawa couplings, *Phys. Rev. D* **102**, 075035 (2020).
- [50] N. Darvishi and M. Krawczyk, CP violation in the extension of SM with a complex singlet scalar and vector quarks, *Nucl. Phys. B* **962**, 115 (2021).
- [51] A. Arsenault, K. Y. Cingiloglu and M. Frank, Vacuum stability in the Standard Model with vector-like fermions, *Phys. Rev. D* **107**, 036018 (2023).

- [52] G. Corcella, A. Costantini, M. Ghezzi, L. Panizzi, G. M. Pruna and J. Šalko, Vector-like quarks decaying into singly and doubly charged bosons at LHC, *JHEP* **10**, 108 (2021).
- [53] Y. Okada and L. Panizzi, LHC signatures of vector-like quarks, *Adv. High Energy Phys.* **2013**, 364936 (2013).
- [54] A. Deandrea, T. Flacke, B. Fuks, L. Panizzi and H. S. Shao, Single production of vector-like quarks: the effects of large width, interference and NLO corrections, *JHEP* **08**, 107 (2021) [erratum: *JHEP* **11**, 028 (2022)].
- [55] A. Carvalho, S. Moretti, D. O’Brien, L. Panizzi and H. Prager, Single production of vectorlike quarks with large width at the Large Hadron Collider, *Phys. Rev. D* **98**, 015029 (2018).
- [56] J. M. Alves, G. C. Branco, A. L. Cherchiglia, C. C. Nishi, J. T. Penedo, P. M. F. Pereira, M. N. Rebelo and J. I. Silva-Marcos, Vector-like singlet quarks: A roadmap, *Phys. Rept.* **1057**, 1 (2024).
- [57] J. F. Kamenik, Y. Soreq and J. Zupan, Lepton flavor universality violation without new sources of quark flavor violation, *Phys. Rev. D* **97**, 035002 (2018).
- [58] N. Arkani-Hamed, A. G. Cohen, E. Katz and A. E. Nelson, The littlest Higgs, *JHEP* **07**, 034 (2002).
- [59] I. Low, W. Skiba and D. Tucker-Smith, Little Higgses from an antisymmetric condensate, *Phys. Rev. D* **66**, 072001 (2002).
- [60] M. Perelstein, M. E. Peskin and A. Pierce, Top quarks and electroweak symmetry breaking in little Higgs models, *Phys. Rev. D* **69**, 075002 (2004).
- [61] S. Chang and J. G. Wacker, Little Higgs and custodial $SU(2)$, *Phys. Rev. D* **69**, 035002 (2004).
- [62] M. C. Chen and S. Dawson, One loop radiative corrections to the ρ parameter in the littlest Higgs model, *Phys. Rev. D* **70**, 015003 (2004).
- [63] T. Han, H. E. Logan and L. T. Wang, Smoking-gun signatures of little Higgs models *JHEP* **01**, 099 (2006).
- [64] J. Hubisz, P. Meade, A. Noble and M. Perelstein, Electroweak precision constraints on the littlest Higgs model with T parity, *JHEP* **01**, 135 (2006).
- [65] C. T. Hill, Topcolor: top quark condensation in a gauge extension of the standard model, *Phys. Lett. B* **266**, 419 (1991).

- [66] C. T. Hill and E. H. Simmons, Strong dynamics and electroweak symmetry breaking, *Phys. Rept.* **381**, 235(2003), [erratum: *Phys. Rept.* **390**, 553 (2004)].
- [67] B. A. Dobrescu and C. T. Hill, Electroweak symmetry breaking via top condensation seesaw, *Phys. Rev. Lett.* **81**, 2634 (1998).
- [68] R. S. Chivukula, B. A. Dobrescu, H. Georgi and C. T. Hill, Top quark seesaw theory of electroweak symmetry breaking, *Phys. Rev. D* **59**, 075003 (1999).
- [69] H. J. He, T. M. P. Tait and C. P. Yuan, New top flavor models with seesaw mechanism, *Phys. Rev. D* **62**, 011702 (2000).
- [70] H. S. Fukano and K. Tuominen, A hybrid 4-th generation: technicolor with top-seesaw, *Phys. Rev. D* **85**, 095025 (2012)
- [71] G. Cacciapaglia, A. Deandrea, N. Gaur, D. Harada, Y. Okada and L. Panizzi, The LHC potential of vector-like quark doublets, *JHEP* **11**, 055 (2018).
- [72] S. Dawson and E. Furlan, A Higgs conundrum with vector fermions, *Phys. Rev. D* **86**, 015021 (2012).
- [73] J. A. Aguilar-Saavedra, R. Benbrik, S. Heinemeyer and M. Pérez-Victoria, Handbook of vector-like quarks: mixing and single production, *Phys. Rev. D* **88**, 094010 (2013).
- [74] C. Y. Chen, S. Dawson and E. Furlan, Vector-like fermions and Higgs effective field theory revisited, *Phys. Rev. D* **96**, 015006 (2017).
- [75] D. Binosi and L. Theussl, JaxoDraw: A graphical user interface for drawing Feynman diagrams, *Comput. Phys. Commun.* **161**, 76 (2004).
- [76] D. Binosi, J. Collins, C. Kaufhold and L. Theussl, JaxoDraw: A graphical user interface for drawing Feynman diagrams. Version 2.0 release notes, *Comput. Phys. Commun.* **180**, 1709 (2009).
- [77] G. C. Branco, L. Lavoura and J. P. Silva, *CP Violation*, Chapter.13(Oxford University Press, New York, 1999).
- [78] G. 't Hooft and M. J. G. Veltman, Regularization and renormalization of gauge fields, *Nucl. Phys. B* **44**, 189 (1972).
- [79] G. 't Hooft, Dimensional regularization and the renormalization group, *Nucl. Phys. B* **61**, 455 (1973).

- [80] G. 't Hooft and M. J. G. Veltman, Scalar one loop integrals, Nucl. Phys. B **153**, 365 (1979).
- [81] G. Passarino and M. J. G. Veltman, One loop corrections for e^-e^+ annihilation into $\mu^+\mu^-$ in the Weinberg model, Nucl. Phys. B **160**, 151 (1979).
- [82] S. A. Larin and J. A. M. Vermaseren, The three loop QCD beta function and anomalous dimensions, Phys. Lett. B **303**, 334 (1993).
- [83] K. G. Chetyrkin, Quark mass anomalous dimension to $\mathcal{O}(\alpha_s^4)$, Phys. Lett. B **404**, 161 (1997).
- [84] J. A. M. Vermaseren, S. A. Larin and T. van Ritbergen, The four loop quark mass anomalous dimension and the invariant quark mass, Phys. Lett. B **405**, 327 (1997).
- [85] T. G. Steele and V. Elias, Pade-improved extraction of $\alpha_s(M_\tau)$ from R_τ , Mod. Phys. Lett. A **13**, 3151 (1998).
- [86] S. Dawson, A. Ismail and I. Low, What's in the loop? The anatomy of double Higgs production, Phys. Rev. D **91**, 115008 (2015).
- [87] L. Wolfenstein, Parametrization of the Kobayashi-Maskawa matrix, Phys. Rev. Lett. **51**, 1945 (1983).
- [88] P. J. Fox, I. Low and Y. Zhang, Top-philic Z' forces at the LHC, JHEP **03**, 074 (2018).
- [89] O. V. Tarasov, A. A. Vladimirov and A. Y. Zharkov, The Gell-Mann-Low function of QCD in the three loop approximation, Phys. Lett. B **93**, 429 (1980).
- [90] K. G. Chetyrkin, B. A. Kniehl and M. Steinhauser, Strong coupling constant with flavor thresholds at four loops in the $\overline{\text{MS}}$ scheme, Phys. Rev. Lett. **79**, 2184 (1997).
- [91] P. A. Baikov, K. G. Chetyrkin and J. H. Kühn, Five-loop running of the QCD coupling constant, Phys. Rev. Lett. **118**, 082002 (2017).
- [92] R. L. Workman *et al.* [Particle Data Group], Review of Particle Physics, Prog. Thro. Exp. Phys **2022**, 083C01 (2022).
- [93] Combined measurements of Higgs boson production and decay using up to $139fb^{-1}$ of proton-proton collision data at $\sqrt{13}$ TeV collected with the ATLAS experiment (2021), <https://cds.cern.ch/record/2789544/>.
- [94] A. Tumasyan *et al.* (CMS Collaboration), A portrait of the Higgs boson by the CMS experiment ten years after the discovery, Nature(London) **607**, 60 (2022).
- [95] C. W. Chiang, X. G. He, F. Ye and X. B. Yuan, Constraints and implications on Higgs FCNC

- couplings from precision measurement of $B_s \rightarrow \mu^+ \mu^-$ decay, Phys. Rev. D **96**, 035032 (2017).
- [96] [ATLAS], Evidence for the $H \rightarrow b\bar{b}$ decay with the ATLAS detector, ATLAS-CONF-2017-041.
- [97] A. M. Sirunyan *et al.* [CMS], Evidence for the Higgs boson decay to a bottom quark-antiquark pair, Phys. Lett. B **780**, 501 (2018).
- [98] H. E. Haber and D. Wyler, Radiative neutralino decay, Nucl. Phys. B **323**, 267 (1989).
- [99] P. Bambade, T. Barklow, T. Behnke, *et al.*, The International Linear Collider: A global project, [arXiv: hep-ex/1903.01629].
- [100] L. Lewin, *Polylogarithms and Associated Functions*(North Holland, New York, 1981), Second Edition.